Journal of Materials Chemistry C

PAPER

The luminescent properties of $CuAlO_2$†

Daragh Byrne,*[a] Aidan Cowley,[b] Nick Bennett[c] and Enda McGlynn[a]

Cite this: *J. Mater. Chem. C*, 2014, **2**, 7859

Received 19th June 2014
Accepted 4th August 2014

DOI: 10.1039/c4tc01311e

www.rsc.org/MaterialsC

In this work we examine the room temperature photoluminescence, Raman and low temperature photoluminescence properties of $CuAlO_2$ prepared using different precursors. At room temperatures the luminescence associated with bulk $CuAlO_2$ occurs at 355 nm and is associated with strong resonant Raman effects. At low temperatures we find that the UV emission is dominated by strong electron–phonon coupling leading to a Franck–Condon type emission band. A second strongly phonon coupled band is also observed in the blue spectral region. In addition we also show that at low temperatures the luminescent properties of $CuAlO_2$ are meta-stable, with anomalous temperature dependence. The possible origins of the blue band, the meta-stability and anomalous temperature dependence are discussed.

1. Introduction

The Delafossite family of compounds are of considerable interest as they have inherent p-type conductivity and, in thin film form, many have high transparencies. Therefore their potential for use in a variety of applications has fuelled research in this area. The first of the Delafossite family of compounds to be proposed for transparent p-type optoelectronic applications was $CuAlO_2$.[1] Consequently much progress has been made in the synthesis/deposition and characterisation of this material. It has been prepared by both relatively low temperature hydrothermal processing and high temperature reactions using either solid state reactions or sol–gel processing.[2–8] Thin films have also been prepared by sputtering, using pulsed laser deposition from $CuAlO_2$ targets made by high temperature methods, and by interfacial reactions.[7–11] Additionally, more exotic methods such as polymer assisted deposition and fungus assisted synthesis have also been demonstrated.[12,13] Despite this rapid advance, many questions remain, particularly with respect to the intrinsic band gap and optical properties of this material. To date, most optical studies have focused on absorption measurements of thin films or single crystals. Many of these studies indicate that $CuAlO_2$ has an indirect bandgap around 2 eV and a direct bandgap *circa* 3.5 eV. However, significant variation in the bandgap values as determined by absorption measurements has been reported, which has generally been ascribed to variations in the processing methods used to produce the material. $CuAlO_2$ has also been the subject of a number of theoretical studies, with varying results obtained for both the direct and indirect transitions. To date, studies of the photoluminescence properties of $CuAlO_2$ have seldom been reported and the reports that are available are limited to room temperature luminescence measurements.[9,12,14–19] At room temperature, thermal effects often obscure important optical properties, which are essential for a comprehensive understanding of a material's properties. Furthermore, determination of the optical properties of a material *via* absorption measurements and Tauc plots can introduce significant error if excitonic effects and surface scattering are important. To address these difficulties we have examined the photoluminescence (PL) and Raman spectroscopic properties of $CuAlO_2$ powders and films made using different precursor materials and have found that the resulting properties are largely identical and reproducible between samples synthesised by different techniques. To further explore the direct bandgap and optically active defects we concentrate on the low temperature luminescence properties of $CuAlO_2$, and our study reveals a number of new and interesting features.

2. Experimental

2.1 $CuAlO_2$ powder

$CuAlO_2$ powder was prepared using the method described in our earlier work.[11] In brief, aluminium isopropoxide was added in small portions to DI-H_2O preheated to 80 °C under vigorous stirring. CuO powder was then added to the resultant Boehmite gel. The excess water and isopropanol by-product were

[a]*School of Physical Sciences, National Centre for Plasma Science and Technology, Dublin City University, Glasnevin, Dublin 9, Ireland. E-mail: daragh.byrne2@mail.dcu.ie; Fax: +353 (0)1 7005384; Tel: +353 (0)1 7005845*

[b]*Nanomaterials Processing Laboratory, Research Institute for Networks & Communications Engineering (RINCE), Dublin City University, Glasnevin, Dublin 9, Ireland*

[c]*School of Engineering and Physical Sciences, Heriot Watt University, Edinburgh, EH14 4AS, Scotland, UK*

† Electronic supplementary information (ESI) available: Sample preparation details for $CuAlO_2$ films on Al_2O_3 and on Cu_2O. SEM images of each of the materials prepared. Raman spectra using 363.8 nm excitation. Low temperature (14.5 K) PL spectra of a $CuAlO_2$ film on a Cu_2O substrate. Details of the peak fitting used to determine the Huang Rhys factor. See DOI: 10.1039/c4tc01311e

evaporated until a semi-solid cake formed. This cake was then transferred to a pre-heated furnace at 1100 °C for 5 hours. After the calcination stage, the cake was removed from the furnace under a nitrogen stream and cooled to room temperature. The excess Cu_xO was then removed by grinding the cake in 36% HCl and filtering, yielding a pale blue, granular powder.

For the majority of low temperature PL study $CuAlO_2$ bulk powder was used. However $CuAlO_2$ films prepared by interfacial reactions between CuO and Al_2O_3 substrates and between Boehmite films coated onto Cu_2O substrates were also examined. Details of the preparation methods used for the films are given in the ESI† and in ref. 11.

2.2 Characterisation

The morphologies and crystal structures of the powders and films were examined using scanning electron microscopy (SEM: Karl-Zeiss EVO series) and X-ray diffraction (XRD: Brucker AXS D8 Advance Texture Diffractometer). Room temperature photoluminescence (PL) measurements and Raman spectra were obtained using the 325 nm line of a HeCd laser coupled to a Jobin Yvon micro-PL spectrometer with no polarisers used either for incident or scattered light. Additional Raman measurements were made using the 488 nm and 363.8 nm lines of an Ar^+ ion laser. Low temperature PL measurements were acquired using the 325 nm line of a HeCd laser and analyzed using a one metre grating spectrometer (SPEX 1704) equipped with a photomultiplier tube (Hamamatsu model R3310-02) cooled to −25 °C.

3. Results and discussion

Given the wide range of optical properties reported for $CuAlO_2$ made using various synthetic methods, we initially examined $CuAlO_2$ made by 3 different (but complementary) methods so as to examine what effect, if any, different precursor materials have on the optical properties. The initial sources of copper ranged from the Cu^{2+} salt copper nitrate, the Cu^{2+} oxide CuO, the Cu^+ oxide Cu_2O while the source of aluminium included α-Al_2O_3 and Boehmite. In each case XRD analysis confirmed the formation of well crystallised $CuAlO_2$ with a low secondary phase content, as shown in Fig. 1. In all cases it was found that the dominant peaks could be indexed to the PDF database card 35-1401, which corresponds to $R\bar{3}M$ $CuAlO_2$ phase, confirming successful material synthesis. Both film-type samples show texture along the [003] axis with respect to the substrate normal, while the powder samples have similar peak intensities to the PDF database entry.

The $CuAlO_2$ films prepared on Cu_2O substrates typically showed weak additional diffraction peaks at 35.5° and 38.7° corresponding to CuO. The relative intensity of the strongest CuO peak at 35.5° as compared to the strongest detected $CuAlO_2$ peak at 36.7° was 0.21. The XRD data from films prepared on polycrystalline Al_2O_3 showed the presence of small quantities of the spinel impurity $CuAl_2O_4$ with a relative intensity of 0.07 as compared to the same $CuAlO_2$ peak. The origins of the spinel impurity are discussed in more detail elsewhere.[11,20] In both

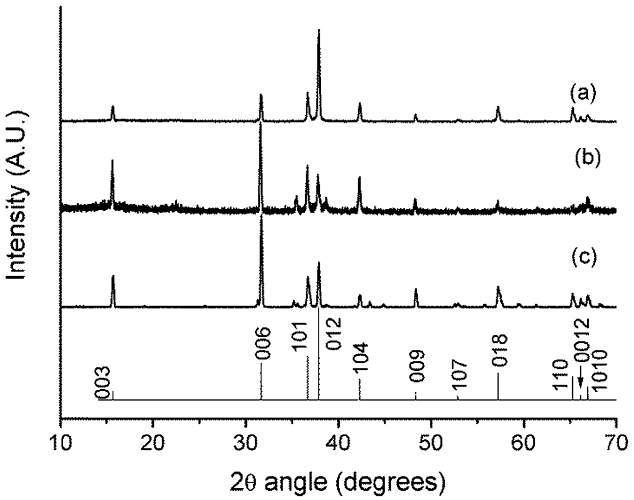

Fig. 1 XRD 2θ-ω scans of $CuAlO_2$ (a) powder and (b) films prepared on Cu_2O substrates as well as (c) films prepared on Al_2O_3 substrates. The trace at the bottom indicates the peak positions expected for the $R\bar{3}M$ $CuAlO_2$ phase (PDF card # 35-1401).

film type samples the strongest peak intensity of the phase impurities corresponded to the strongest peak intensity of their corresponding PDF database entry. Given the texture of the $CuAlO_2$ was along an axis which has approximately halve the maximum peak intensity, the relative peak ratios may overestimate the phase impurities present. The $CuAlO_2$ powders prepared with an excess of CuO were found to be phase pure. SEM data (ESI S1†) reveal that the powders consisted of a mixture of small nanocrystals (~100 nm), larger aggregates and large (~50 μm) well defined crystals. Films prepared on Al_2O_3 consist of smaller nm scale crystals (~50 nm) and larger well defined crystal structures (~30 μm), while samples prepared on Cu_2O consist of large flat platelets composed of aggregates of smaller nanocrystals.

3.1 Raman spectra

The 4 atom primitive cell of $CuAlO_2$ leads to 12 normal vibrational modes at the Brillouin zone centre which can be categorised by symmetry labels as follows: $\Gamma = A_{1g} + E_g + 3A_{2u} + 3E_u$. Only the A_{1g} and E_g modes are Raman active.[21,22] Room temperature Raman spectra acquired using a 488 nm laser, shown in Fig. 2, consists of two main peaks located around 418.9 ± 0.5 cm^{-1} and 767.5 ± 0.5 cm^{-1} corresponding to the E_g and A_{1g} modes, and these positions agree well with the previously calculated (433 cm^{-1} and 770 cm^{-1}) and experimentally determined values for high quality $CuAlO_2$ single crystals (418.1 cm^{-1} and 767.2 cm^{-1}).[21] The appearance of both modes in the backscatter geometry is due to the polycrystalline nature of the samples examined. With the micro-Raman system used in this study, individual crystallites could be examined across the various different materials. This revealed small shifts in the Raman peak positions both between samples and from various different crystallites within the same sample. Therefore more precise positions for each of the allowed modes could not be

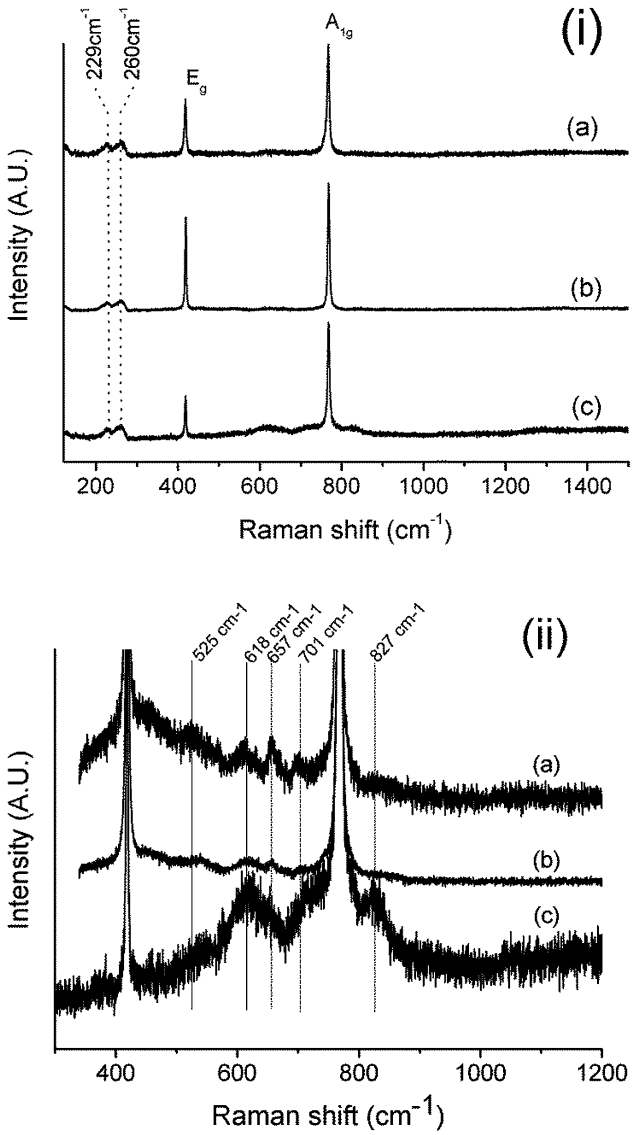

Fig. 2 Room temperature unpolarised Raman spectrum using 488 nm excitation by an Ar^+ laser. $CuAlO_2$ (i) full spectrum (ii) magnified intensity axis, where the various traces indicate material source: (a) $CuAlO_2$ powder (b) $CuAlO_2$ film on Cu_2O (c) $CuAlO_2$ film on Al_2O_3.

determined, nor were any clear trends observed in terms of the shift with respect to the crystallite size or morphology. Previously it has been observed that in $CuAlO_2$, the degree of excess interstitial oxygen leads to a distortion of the crystal lattice structure which can be subsequently observed as a shift in the Raman peak position.[22] The difference in peak positions observed across samples and between samples may therefore in part be due to a natural variation in the excess oxygen interstitials or other defects, in combination with residual stress from the high temperature synthesis. The presence of impurities may also contribute to small shifts observed, however, at present we do not have any clear indication that this is the dominant cause. In addition to the strongly allowed modes, a closer examination of the baseline region of the spectra (Fig. 2(ii)) revealed a number of additional weak peaks centred around 229, 260, 525, 618, 657 and 701 cm^{-1}. As with the shift in allowed modes, no definitive correlation could be established between the impurity phases detected in the XRD spectra and the additional peaks observed in the Raman spectra. The dominant impurity in the film prepared on Cu_2O was CuO which has Raman peaks at centred around 297, 344 and 631 cm^{-1}.[23] The spinel impurity $CuAl_2O_4$ observed in XRD spectra of the samples prepared on Al_2O_3 would be expected to yield Raman peaks around 356, 450, 595, 698 and 767 cm^{-1}.[24] While some of the additional peaks identified may indeed have contributions from the impurity phases present, the closest match in terms of peak spectral position is to that of the L-series, as identified by the study of Pellicer-Porres *et al.* of high quality single crystal $CuAlO_2$.[21] (The positions from ref. 21 are: L2: 227 cm^{-1}, L3: 262 cm^{-1}, L6: 524 cm^{-1}, L7: 617 cm^{-1}, L8: 659 cm^{-1}, L9: 712 cm^{-1}.) The L-series are believed to arise from the presence of forbidden non-zero wavevector phonons modes which suggest a disruption of the crystal translational symmetry leading to a relaxation of the Raman selection rules, indicative of the presence of defects in the crystal structure. Similar forbidden modes have been observed in other Delafossite compounds and may have similar origins, *e.g.* interstitials, vacancies and substitutional defects.[25] One notable exception is that of the sample prepared on Al_2O_3 where some of the crystallites examined showed a significantly larger increase in the L7 peak located at ~618 cm^{-1} compared to the other samples examined and also showed a secondary weaker peak at ~1267 cm^{-1}. As is discussed later, this sample had significantly different low temperature luminescence properties.

3.2 Room temperature PL and resonant Raman spectra

Banerjee *et al.* first reported luminescence data from $CuAlO_2$ which consisted of a single broad peak centred around 348.5–399 nm, the exact position of which depended on the particle size, as strong quantum confinement effects were observed.[9,15] Since then there have been only a few reports on the luminescent properties of $CuAlO_2$, with peak emissions ranging from 350–500 nm but more typically 350–400 nm.[12,14,16–19,26] In terms of defect emission, only two reports could be found in the literature indicating the presence of defect luminescence, again with significantly different peak positions being reported. In the spectra reported by Chiu *et al.* an additional emission centred around 428 nm was observed, while Fang *et al.* observed two additional bands at 470 nm and 590 nm ascribed to copper vacancies and interstitial oxygen respectively.[17,18] Therefore, before examining the low temperature photoluminescence spectra, we first examined the PL properties of our samples at room temperature. Using the 325 nm line of a HeCd laser as an excitation source allowed us to capture the Raman signal and photoluminescence signals simultaneously.

Fig. 3 shows PL spectra taken at room temperature. The first point to note is that at room temperature no defect emissions were detected up to 600 nm. As with the Raman spectra, the dominant PL emission was found to vary in position and in intensity both between samples and between individual crystallites of the same sample, with the peak lying between 353 nm

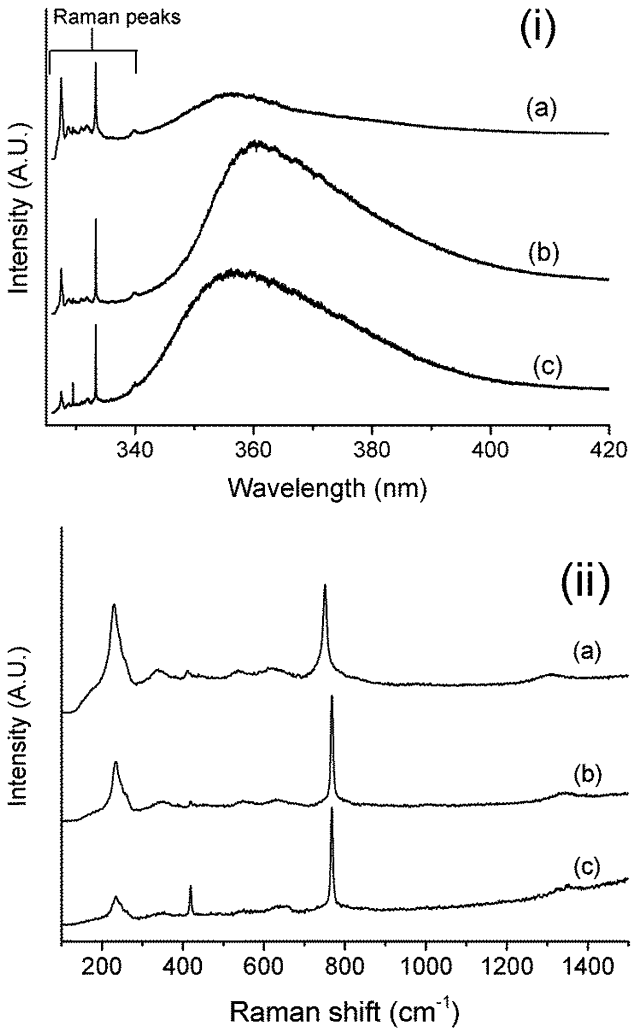

Fig. 3 (i) Room temperature photoluminescence and near resonant Raman spectra of $CuAlO_2$ (ii) resonant Raman spectra of $CuAlO_2$. (a) Powder (b) film on Cu_2O (c) film on Al_2O_3. All spectra have been normalised in intensity to the A_{1g} Raman signal at 333.3 nm.

and 366 nm. No spectra exhibited peak emission intensities beyond these limits. Similar shifts in the position of PL peaks at room temperature have previously been observed in $CuAlO_2$ and in other materials. The origin of these shifts is generally poorly understood and has been ascribed to various effects such as non-uniform heating from the focused laser spot, quantum confinement, stress/strain or Fröhlich interactions.[15,27,28] In addition, the presence of secondary phases may also have unresolved contributions leading to small shifts in the overall peak positions. This latter possibility was examined in further detail given that the film samples showed some evidence of impurities. No luminescence signal which could contribute to the peak shift was observer for CuO or Cu_2O. The Al_2O_3 substrate was found to have a broad luminescence across the visible spectrum. The closest band to the region of interest was centred around 390 nm which if present in $CuAlO_2$ could contribute to the red shift in the UV band. However, the emission at 390 nm was strongly quenched when the Al_2O_3 substrate was doped with Cu. Powders prepared under sub-optimal conditions which were rich in impurities such as CuO, $CuAl_2O_4$, Al_2O_3 typically had little or no luminescence. The 390 nm Al_2O_3 emission was not observed in conjunction with the $CuAlO_2$ band. Given that the luminescence was collected using a tightly focused spot, the possibility of small contributions from unreacted Al_2O_3 which was not detected by XRD or Raman, should not be discounted. The observation of shifts in the peak position even with the same batch of material highlights the difficulties in interpreting room temperature measurements and underscores the importance and motivation for detailed low temperature studies. Given the proximity of the laser wavelength to the material bandgap, the 325 nm excitation source was found to significantly increase the intensity of the non-zero wavevector phonon Raman lines *via* resonance effects which can easily be discerned in the spectra shown in Fig. 3(i) and shown in more detail in Fig. 3(ii). Previously Banerjee *et al.* reported strong quantum confinement in $CuAlO_2$ nanoparticles leading to a blue shift in the room temperature PL emission.[15] In this study, large well defined crystallites were examined in conjunction with smaller crystallites and we see no evidence that quantum confinement plays a role in the distribution of peak positions in our samples. The spectra in all cases had a broad full width at half maximum (FWHM) ranging from 30 nm to 40 nm. However, in some instances the PL intensity was too weak to measure an accurate FWHM, so the upper value may be higher. For most samples which showed reasonably strong luminescence, the spectra showed a pronounced resonance enhanced Raman peak centred around 236.5 cm^{-1}. The only exception to this general observation was that if the E_g peak at $\sim$418 cm^{-1} was strong then the 236.5 cm^{-1} peak was attenuated (an example of which is seen by comparing in Fig. 4(a) with 4(b)). This effect can also be seen in trace (c) of Fig. 3(ii).

The E_g mode was observed in all samples using a 488 nm excitation source. However, at lower excitation wavelengths (and in this instance close to the direct bandgap energy) the penetration depth is reduced and surface scattering will contribute more to the Raman signal leading to a reduction in

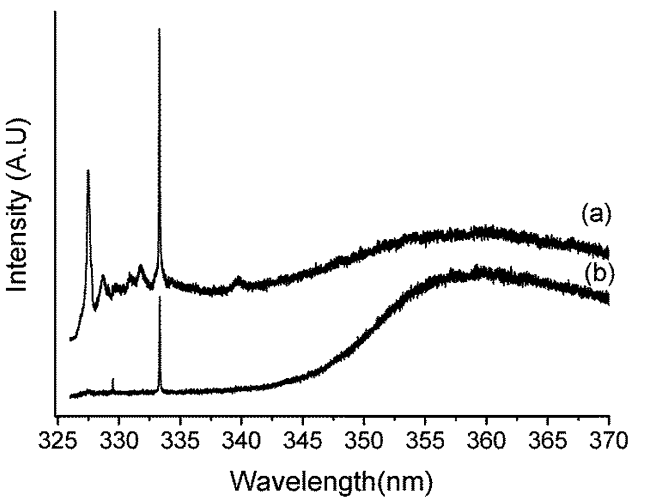

Fig. 4 Room temperature PL and resonant Raman spectrum of $CuAlO_2$ (a) showing a weak E_g mode (b) showing a strong E_g mode.

the E_g mode. The increase in the intensity of the E_g mode seen in some crystallites therefore indicates that the orientation of the crystal being examined at least partially satisfied the selection rule for this mode.[21] Specifically, observation of the E_g mode in Raman requires that the *c*-axis of the crystal under examination must not be parallel to the incident beam, and this condition is satisfied to varying degrees by different crystals. Given that the orientation of the crystal with respect to the incident laser could be identified by the intensity of the E_g mode and that the peak located at 236.5 cm^{-1} was strongly suppressed in orientations where the E_g mode scattering is strong, it appears that the peak at 236.5 cm^{-1} has an angle-dependent scattering cross-section. All materials were examined for resonance Raman effects using a (sub-bandgap) 363.8 nm laser line as the excitation source (ESI S2†), where it was found that the spectra, including the strong scattering at ~236 cm^{-1} under 325 nm illumination, were reduced in intensity and therefore were nearly identical to those obtained under 488 nm illumination. These two observations suggest that 236.5 cm^{-1} peak may be associated with intrinsic crystalline vibrational modes as opposed to defect modes where isotropic scattering and resonance effects at sub-bandgap excitation energies might be expected.[29] The identity of the peak at 236.5 cm^{-1} has yet to be identified, and further studies are required to conclusively confirm the origins of the near resonance enhanced Raman peaks. However, strong electron–phonon interactions can be indicative of a localised exciton, forming a polaronic-type state. Notwithstanding the small variations observed between individual crystallites, the similarities displayed across the XRD, Raman and photoluminescence data at room temperature for the $CuAlO_2$ samples made by the different methods lead us to conclude that the properties of the materials produced are largely similar and independent of the choice of precursor materials. The natural variation observed in the optical properties seen between individual crystallites does however serve to highlight the challenges in producing uniform material.

3.3 Low temperature photoluminescence

Fig. 5 shows low temperature PL spectra of $CuAlO_2$ powder, measured at 14.5 K. The sharp peak at 368 nm is due to a laser plasma line. No additional peaks were observed for wavelengths greater than 500 nm, however we also note that the sensitivity of the system used in this study is reduced at longer wavelengths. In all samples examined, the PL spectra were found to consist of two broad bands centred around 355 nm and 430 nm respectively. At the highest resolution obtainable (<0.5 nm), both bands could not be further resolved into clearly distinct peaks, however both the UV and blue bands showed a fine structure on the high energy side which can be seen in greater detail in Fig. 5(b). The same features were observed for the samples produced by the interfacial reaction of Boehmite coated on a Cu_2O substrate an example of which is shown in the ESI S3.† Both the position of the UV and blue bands, the presence of a fine structure on the high energy side and the band FWHM were comparable. While the ratio of the integrated area of the two bands between the film sample and powder were similar, some

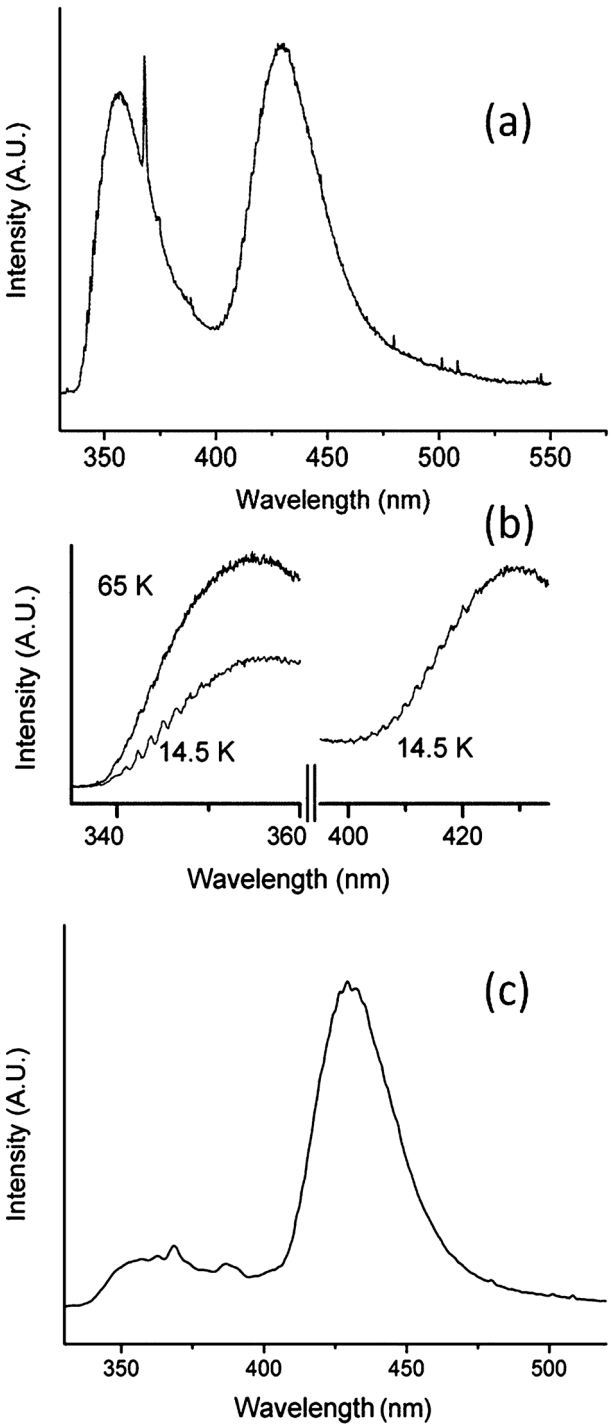

Fig. 5 (a) Typical high resolution PL spectra of $CuAlO_2$ at 14.5 K. (b) Magnification of the UV band and blue band fine structure at 14.5 K and 65 K. (c) Low resolution PL spectra obtained for $CuAlO_2$ on Al_2O_3.

variations were observed. However, as shall be discussed shortly the relative intensity of the bands was found to be dependent on the measurement duration/illumination time. The film sample prepared by the interfacial reaction between Al_2O_3 substrate and CuO also shared many similar features in that the same two bands were clearly identifiable. The overall PL intensity was significantly weaker, forcing us to measure this sample at lower

resolutions. While the band positions remained the same for this sample, as can be seen in Fig. 5(c) the relative intensity of the blue band was significantly stronger than that of the UV band. Given that each of the different types of samples examined at low temperature and had largely equivalent properties in terms of the position of the bands observed, we shall confine the bulk of our discussion to the spectra from the phase pure powder samples which are broadly representative of the sample set. The anomalous spectra obtained for the film sample on Al_2O_3 as shown in Fig. 5(c) is discussed in more detail in Section 3.3.2.

3.3.1 UV emission. As far as we are aware the low temperature PL spectrum of $CuAlO_2$ has not previously been reported and therefore direct comparison to other findings is not possible. PL studies of other Delafossite compounds such as $CuLaO_2$ and $CuYO_2$ share some qualitative similarities in that two emission bands are observed in such materials with the lower wavelength emission quenching rapidly with rising temperature.[30] From a combination of PL and excitation measurements of the Delafossite $CuLaO_2$ and $CuYO_2$, it was concluded that the shorter wavelength emission is due to the hybridised $\delta(3d_z^2 - 4s) \rightarrow \delta^*(3d_z^2 + 4s)$ transition on the Cu ion while the longer wavelength band is due to a $\delta(3d_z^2 - 4s) \rightarrow 3d^9 4p^1$ transition on the Cu ion with a larger Stokes shift. For $CuAlO_2$, more recent calculations suggest that the Cu 3d level is modified by the O 2p orbitals, creating closely spaced maxima at the F and L points in the Brillouin zone, with the L point yielding the lowest direct transition.[31–34]

The calculated values for the direct band gap range from 3 to 4 eV while the experientially determined bandgaps typically yield a value of ~3.5 eV.[31,32,34–36] In this work the emission peak associated with the direct bandgap was located at 355 ± 2 nm (3.49 eV) at 14.5 K While this figure is in good agreement with the earlier reports from room temperature photoluminescence and absorption measurements, the presence of a fine structure implies a somewhat more complex picture. Typically at low temperatures and in the absence of strong electron–phonon coupling, one would expect a reduction in the peak FWHM in the case of free exciton emission, as both the phonon contribution to broadening as well as the kinetic energy of the free particle reduces. This was not the case in the present study for the UV emission where the FWHM was typically ~34 nm, similar to the room temperature measurements. Despite the large range of samples examined, the temperature dependent measurements and power dependent measurements, failed to show any evidence that the UV emission may have strong secondary hidden bands which contribute to the broad emission. However, in some circumstances, a weak unresolvable shoulder was observed on the low energy side of the dominant UV band. The observation of a fine structure, is consistent with a localised excitation with strong-electron–phonon coupling leading to a vibronic Franck–Condon emission band. In such cases it is common to examine the emission spectrum within the framework of the configuration coordination model. For the simplest case within the configuration coordinate model, the linear coupling regime, where the force constants of the ground and excited state are equal and approximated by a harmonic oscillator, the spectrum can be modelled as a Franck–Condon series given by an expression of the form:

$$I_\omega = A \sum_{n=0}^{\infty} e^{-S} \frac{S^n}{n!} \delta(\omega - \omega_{eg} - j\omega_0)$$

where S, the dimensionless Huang Rhys factor, relates the strength of coupling to the nuclear degrees of freedom, δ is the line shape function of the individual transitions within the overall envelope, ω_{eg} is the zero-phonon energy and ω_0 is the phonon energy. The Huang Rhys factor can then be estimated from this function by fitting the intensity ratio of successive phonon modes. Details of the fitting procedure are given in the ESI.† For the UV emission it was found that the Huang Rhys factor was ~8.7 ± 1.2 which represents a very strong coupling between the excited state and the lattice. However some caution must be applied because the above expression predicts that if all the assumptions of the one dimensional configuration coordinate model are fully satisfied the PL band shape should be symmetric and in the form of a Poisson distribution. In the case of $CuAlO_2$ the UV band has an asymmetric shape with low energy tail and this behaviour is associated with the quadratic coupling regime where the ground and excited state have different force constants.[37] The secondary weak emission observed under photo-bleaching conditions (mentioned above and discussed later) may also contribute to the asymmetric tail. Similar to other phonon-replica structured bands, as the temperature is raised the phonon peaks begin to broaden. By 65 K they are barely discernible and beyond that temperature, no longer resolvable. The zero phonon position line could not be observed however it is expected to be located around 337.3 ± 1.3 nm giving $CuAlO_2$ a low temperature optical band gap of 3.68 eV. The average phonon peak spacing is ~1.3 nm (125 cm^{-1}, 14 meV) however the overlap of closely spaced of the phonon replicas due to broadening leads to some variation across the set of resolved phonon replica peaks. Unfortunately, this phonon energy was beyond the range measurable with our Raman system, due to its proximity to the Rayleigh-scattered laser line. It has been reported that Cu fluorescence involving the $3d^9 4s \rightarrow 3d^{10}$ is strictly forbidden in the free ion but partially allowed in solids *via* coupling to lattice vibrations of odd parity.[38] In addition the direct transition is believed to occur at the L point in the Brillouin zone. The phonon replica may then correspond to the L1 peak (119 ± 5 cm^{-1}) observed by Pellicer-Porres *et* al. whose closest match was the B_{1u} (X) or A_{1g} (L) mode, in good agreement with mode observed here.

3.3.2 Blue emission. The blue emission band found in all samples varied in intensity with respect to the UV emission, typically ranging from slightly weaker to significantly stronger. For the majority of samples examined the initial intensity of the blue emission was of similar intensity to that of the UV emission. As with the UV band, the blue band also had a resolvable fine structure on the high energy side with a phonon spacing of ~1.95 nm (185 cm^{-1}, 27 meV).

As mentioned earlier, previous optical studies of the Delafossite compounds $CuLaO_2$ and $CuYO_2$ have also detected a second emission band which was assigned to $\delta(3d_z^2 - 4s) \rightarrow$

$3d^9 4p^1$ transition with a larger Stokes shift.[30] The second band in $CuLaO_2$ and $CuYO_2$, despite appearing at longer wavelengths in PL, actually corresponds to a higher energy transition to the $4p_xp_y$ orbital with a large Stokes shift resulting in an emission band below that of the near band-edge emission. Some qualitative similarities exist between the blue emission seen in $CuAlO_2$ and the low energy bands seen in $CuLaO_2$ and $CuYO_2$ in that (i) it is readily quenched by heating and (ii) its position is at energies below the fundamental excitonic transition. Furthermore, the Stokes shift of the $\delta(3d_z^2 - 4s) \rightarrow 3d^9 4p^1$ transition was predicted to decrease as the size of the trivalent metal atom reduces, which is consistent with the observation of both the blue and UV emission band in $CuAlO_2$ with a 325 nm excitation source. In this scenario the ZPL position for the blue band in $CuAlO_2$ would lie above the UV transition (~337.3 nm) and below the excitation source (325 nm) and would therefore have a Huang Rhys factor of between 47 and 54. An exacting fit to the ratio of phonon peak replicas is challenging owing to the uncertainty induced by the overlapping bands and the strong influence of small variations in the UV band tail to any fit of the ratio of successive phonon modes. As a result, an accurate value for the ZPL position and Huang Rhys factor cannot not be determined for this band at present, based on this model.

We must however also consider other possible origins for the blue emission, particularly given that in some of the samples examined in this work, a strong variation in the blue band intensity seemed related to the annealing steps used and this behaviour is more indicative of defect-related radiation. Fig. 5(c) shows the PL spectrum of a $CuAlO_2$ film on Al_2O_3 which during its preparation was annealed a second time for three hours at 1100 °C. Prior to annealing the $CuAlO_2$ film was black in colour and had exceptionally weak room temperature photoluminescence. After annealing the sample had changed to a grey colour, and its room temperature luminescence properties showed some improvement. At low temperatures, compared to the spectra typically obtained for materials prepared by a single annealing step, the UV emission was attenuated and blue emission was significantly enhanced. Previously it has been shown that annealing $CuAlO_2$ films leads to an enhancement in the electrical properties and appreciably alters the optical transmission.[39,40] The conduction mechanisms in $CuAlO_2$ have been the subject of much debate. Ingram *et al.* proposed a small polaron hopping mechanism.[3,41] Lan *et al.* found that above 190 K the conductivity was thermal activated while below this temperature the conductivity was due to a variable range hopping mechanism.[42] More recently an acceptor defect level located 700 meV above the valence band has been identified.[4] The theoretical analysis of Scanlon et *al.* indicate that the dominant defects are Cu_{Al} and V_{Cu}; with V_{Cu} forming an acceptor level at 680 meV.[34] Given that the optical bandgap determined in this work is ~3.68 eV, then a transition from the zero vibrational level excited state to the acceptor level may then be expected around 2.98 eV, close to the peak emission of the blue band at (2.88 eV). The enhancement in conductivity *via* thermal annealing may then in part result from the formation of more V_{Cu} defects. It follows from these observations, along with the significant increase in the blue band intensity post annealing, that a second possible and plausible origin for the blue band is a transition involving an acceptor level ~800 meV above the valence band which may be related to V_{cu} or another thermally induced defect. More detailed knowledge of the ZPL position for this band should yield a value closer to those previously reported.

Both possible origins discussed here raise further interesting questions. If the blue band is due to a higher energy transition with larger stokes shift, what leads to the increase in blue emission in some samples? Or if the band is due to defects such as V_{Cu} what are the origins of the defect bands previously observed at room temperature?

3.3.3 Meta-stability and temperature dependent luminescence. At low temperatures, for all materials examined, the UV and blue emission intensity showed meta-stability effects, with the peak and integrated intensity changing significantly over time. An illustration of this can be seen in Fig. 6(a) where the integrated peak area of both bands over the course of a 17 hour period at 14.5 K are shown. Prior to measurement, the sample had been held at 14.5 K for approximately 12 hours. During the course of measurements the UV emission had a near linear reduction in the peak area. After 17 hours the emission reduced to ~40% of it's initial value. The blue emission initially increased (reaching a maximum after ~3.5–5 hours) before declining again. After 9 hours a clear reduction in the blue emission is observed, reaching its initial value and decreasing by 30% of its initial intensity after 17 hours. The laser plasma line intensity was also measured to provide an excitation intensity reference and was found to be quite stable during the course of the experiment showing a variance of <9%. Furthermore the effects of drift in laser power can be excluded as a factor given that power dependent measurements (Fig. 6(d)) show that both bands have a k value of ~1 where k is the exponent in the dependence of the emission intensity on excitation power and therefore the peak intensities are directly proportional to the excitation intensity. In these measurements, the intensity of the blue emission was seen to increase before decreasing, while the UV emission showed a monotonic decrease.

The rise time of the blue emission appeared to vary between samples but a rise in intensity occurred in all samples examined and therefore appeared to be a universal property of the $CuAlO_2$ materials examined in this study. During the course of illumination, the band FWHM and band peak positions remained largely constant. Only minor variations in the bands FWHM were observed, while the band peak positions shifted by less than a single phonon mode spacing. To further examine the band meta-stability, temperature dependent measurements were performed on heavily photo-bleached samples and rapidly cooled samples. Fig. 6(b) shows the temperature dependence of the integrated peak areas for both bands from a heavily photo-bleached sample which was achieved by illuminating the sample for ~24 hours with the excitation source prior to measurement. Between 14 and 25 K the blue emission decreased sharply while the UV emission stayed approximately constant. Beyond 25 K the PL intensity for both emissions increased rapidly reaching a peak at ~50 K. From 50 K on, the

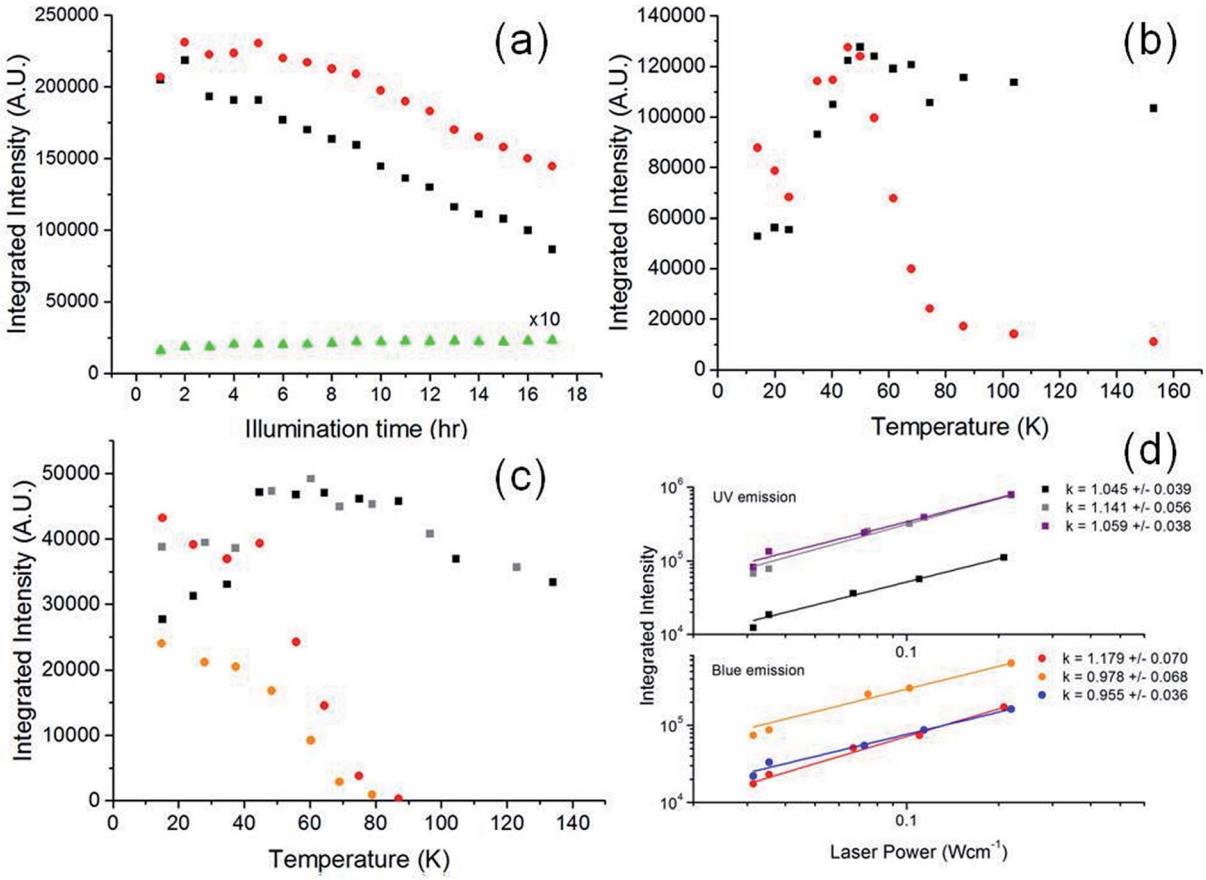

Fig. 6 (a) Variation of integrated peak area over time at 14.5 K, (UV band: black square; blue band: red circle; laser plasma line: green triangle). (b) Temperature dependant PL of a heavily bleached sample; (UV band: black square; blue band: red circle). (c) Temperature dependent PL of a lightly bleached and deliberately non-bleached sample, (UV band lightly bleached: black square; UV band non-bleached: grey square; blue band lightly bleached: red circle; blue band non-bleached: orange circle). (d) Power dependant PL at 14.5 K and 65 K, (UV band bleached: black square; UV band non-bleached: grey square; UV band at 65 K: purple square; blue band bleached: red circle; blue band non-bleached: orange circle, blue band at 65 K: blue circle).

blue emission decayed quickly, whilst UV emission intensity reduced but at a considerably slower rate. From these results we can draw a number of important conclusions. Firstly, the metastability, while manifesting itself slightly differently in each band was clearly identifiable in both bands. Secondly, temperature dependent measurements after photo-bleaching showed that the luminescence for both bands reached a maximum at 50 K. This similarity in properties clearly indicates that both the bands are due to the $CuAlO_2$ crystal and not due to the presence of secondary phases undetected by XRD or Raman spectroscopy. Furthermore, the peak intensity for both bands coincided at 50 K, which strongly suggests that the photo-bleaching effect observed in both bands has a common origin. The anomalous temperature dependent behaviour was also seen in samples which were not pre illuminated. Fig. 6(c) shows a comparison of the thermal response between a moderately photo-bleached sample and one for which efforts were made to inhibit photo-bleaching, by rapidly cooling the sample from above 65 K to 14 K in under 20 minutes, using short measurement times and turning off all illumination between measurements while temperature adjustments were made. The lightly bleached sample showed the same trends as the heavily bleached in that both bands peaked at 50 K after which the blue band rapidly decreased, while the UV band slowly declined. The UV emission for the sample where efforts to prevent bleaching were made showed broadly similar trends in that the luminescence intensity for the UV band increased from its initial 14 K value, reaching a maximum at 50 K. The behaviour of the blue band displayed a somewhat different trend given that the intensity only quenched as the temperature increased. However, the rate of quenching increased to match the bleached sample for temperatures greater than 50 K. This difference in behaviour between the UV and blue bands confirms the earlier observations with respect to the variation of bands with illumination time and suggests that the UV band is initially more susceptible to bleaching.

Power dependent measurements were made for all three cases, *i.e.* for the bleached, non-deliberately bleached and samples 15 K above the 50 K transition temperature. In all cases both bands were found to have a linear relationship between illumination and luminescence intensity in the power range examined and could be well fitted to the power law $I \sim P^k$. The k

value obtained for the UV emission was 1.0, 1.1 and 1.1 while the k values for the blue emission was 1.2, 1.0 and 1.0 for the bleached, non-bleached and 65 K measurements, respectively.

As far as we are aware, the luminescence emission meta-stability observed in this work has not been reported in other Delafossite compounds. However the features observed bear similarities to the meta-stability observed in Cu^{+1} doped β″-alumina.[43] Cu^{+} doped β″-alumina consists of dense alumina planes separated by a Cu^{+1} conduction plane. In these materials it has been found that the cations within the conduction plane are highly mobile and the Cu^{+} ions can form $(Cu_2)^{+2}$ dimers. Furthermore, dimer formation can be enhanced under UV illumination if the dimer is stabilised in the excited state.[38,43] At low temperatures, this mobility and dimer formation leads to dynamic luminescence behaviour. Cations moving to new locations and/or forming dimmers leads to the quenching of the monomer Cu^{+} emission and the emergence of dimer emissions within relatively rapid timescales. Cu^{+}–Cu^{+} interactions are known to play an important role in many Cu^{+1} compounds and in the bandgap, conductivity and transparency of $CuAlO_2$.[44–46] Therefore, any disturbance in the Cu^{+} interactions such as the formation of dimmers or trimers with neighbouring or interstitial Cu atoms could lead to a situation analogous to Cu^{+} doped β″-alumina. The longer timescales necessary to observe the photo-bleaching effect in $CuAlO_2$ as compared to Cu^{+} doped β″-alumina (minutes *versus* hours), can be interpreted in terms of the reduced ion mobility within the conduction plane or reduced probability of neighbouring Cu^{+}–Cu^{+} interactions. On close inspection of the spectra during bleaching, a new weaker shoulder is seen to emerge on the low energy side of the UV emission (ESI S6†). Whether this shoulder is related to the bleaching or merely revealed owing to the bleaching of the dominant UV emission has yet to be determined. However, given that Cu^{+}–Cu^{+} dimers have been directly observed in other materials, it may be that Cu^{+}–Cu^{+} interactions in $CuAlO_2$ leads to additional spectral features. While the meta-stability is most likely due to the low temperature photochemistry, it is curious to note that the temperature at which the onset of meta-stability occurs coincides closely with the, albeit disputed, superconductivity transition temperature in $CuAlO_2$.[47–49] What effect if any, UV illumination at low temperatures has on the electrical properties is yet to be examined but shall be the focus of further studies.

4. Conclusions

At a constant processing temperature during synthesis, we find that the optical properties of $CuAlO_2$ grown by different techniques to be largely consistent, irrespective of the precursor materials used and XRD and Raman data indicate that the properties of the materials examined are largely consistent with previous reports. At room temperature, $CuAlO_2$ shows a single PL emission band, which after examination at low temperatures has been shown to result from a strongly coupled Franck–Condon progression with a Huang Rhys Factor of $\sim 8.7 \pm 1.2$ corresponding to an optical bandgap of 3.68 eV. A second blue band also appears at low temperatures which also has strong electron–phonon coupling, though the exact coupling strength was not deducible from our data due to overlap with the UV emission band tail. The possible origins of this band include a transition to a higher energy level with a large Stokes shift or a defect level induced by defects such as Cu vacancies. Both UV and blue emission bands show meta-stability effects and anomalous temperature dependence, which persists up to 50 K. Beyond this temperature the blue band rapidly decays indicating a small activation energy, while the UV emission persists to room temperature. At present we believe the meta-stability is most likely related to the photochemistry and more specifically to possible Cu–Cu interactions. However, further work is required to confirm this preliminary assignment.

Acknowledgements

DB, AC and NB wish to acknowledge the assistance of Royal Society International Exchange Scheme grant IE131212.

Notes and references

1 H. Kawazoe, M. Yasukawa, H. Hyodo, M. Kurita, H. Yanagi and H. Hosono, *Nature*, 1997, **389**, 939–942.
2 D. Y. Shahriari, A. Barnabè, T. O. Mason and K. R. Poeppelmeier, *Inorg. Chem.*, 2001, **40**, 5734–5735.
3 B. J. Ingram, G. B. González, T. O. Mason, D. Y. Shahriari, A. Barnabè, D. Ko and K. R. Poeppelmeier, *Chem. Mater.*, 2004, **16**, 5616–5622.
4 J. Tate, H. L. Ju, J. C. Moon, A. Zakutayev, A. P. Richard, J. Russell and D. H. McIntyre, *Phys. Rev. B: Condens. Matter Mater. Phys.*, 2009, **80**, 165206.
5 Z. Deng, X. Zhu, R. Tao, W. Dong and X. Fang, *Mater. Lett.*, 2007, **61**, 686–689.
6 J. Ding, Y. Sui, W. Fu, H. Yang, S. Liu, Y. Zeng, W. Zhao, P. Sun, J. Guo, H. Chen and M. Li, *Appl. Surf. Sci.*, 2010, **256**, 6441–6446.
7 J. H. Shy and B. H. Tseng, *J. Phys. Chem. Solids*, 2008, **69**, 547–550.
8 J. H. Shy and B. H. Tseng, *J. Phys. Chem. Solids*, 2005, **66**, 2123–2126.
9 A. N. Banerjee and K. K. Chattopadhyay, *J. Appl. Phys.*, 2005, **97**, 084308.
10 M. Neumann-Spallart, S. P. Pai and R. Pinto, *Thin Solid Films*, 2007, **515**, 8641–8644.
11 D. Byrne, A. Cowley, P. McNally and E. McGlynn, *CrystEngComm*, 2013, **15**, 6144–6150.
12 A. Ahmad, T. Jagadale, V. Dhas, S. Khan, S. Patil, R. Pasricha, V. Ravi and S. Ogale, *Adv. Mater.*, 2007, **19**, 3295–3299.
13 H. M. Luo, M. Jain, T. M. McCleskey, E. Bauer, A. K. Burrell and Q. X. Jia, *Adv. Mater.*, 2007, **19**, 3604–3607.
14 T. Prakash, K. P. Prasad, S. Ramasamy and B. S. Murty, *J. Nanosci. Nanotechnol.*, 2008, **8**, 4273–4278.
15 A. N. Banerjee, S. W. Joo and B.-K. Min, *J. Appl. Phys.*, 2012, **112**, 114329.
16 H.-Y. Chen and M.-W. Tsai, *Thin Solid Films*, 2011, **519**, 5966–5970.

17 S. H. Chiu and J. C. A. Huang, *Surf. Coat. Technol.*, 2013, **231**, 239–242.
18 M. Fang, H. He, B. Lu, W. Zhang, B. Zhao, Z. Ye and J. Huang, *Appl. Surf. Sci.*, 2011, **257**, 8330–8333.
19 R. Mo and Y. Liu, *J. Sol-Gel Sci. Technol.*, 2011, **57**, 16–19.
20 A. P. Amrute, Z. Łodziana, C. Mondelli, F. Krumeich and J. Pérez-Ramírez, *Chem. Mater.*, 2013, **25**, 4423–4435.
21 J. Pellicer-Porres, D. Martinez-Garcia, A. Segura, P. Rodriguez-Hernandez, A. Munoz, J. C. Chervin, N. Garro and D. Kim, *Phys. Rev. B: Condens. Matter Mater. Phys.*, 2006, **74**, 184301.
22 W. Lan, J. Q. Pan, C. Q. Zhu, G. Q. Wang, Q. Su, X. Q. Liu, E. Q. Xie and H. Yan, *J. Cryst. Growth*, 2011, **314**, 370–373.
23 Y. Dongliang, G. Chuannan and D. Youwei, *J. Semicond.*, 2009, **30**, 072003.
24 N. Tomar, E. Ghanti, A. K. Bhagi and R. Nagarajan, *J. Non-Cryst. Solids*, 2009, **355**, 2657–2662.
25 O. Aktas, K. D. Truong, T. Otani, G. Balakrishnan, M. J. Clouter, T. Kimura and G. Quirion, *J. Phys.: Condens. Matter*, 2012, **24**, 036003.
26 Q. Lin, F. Miao and Y. Huang, *Appl. Mech. Mater.*, 2014, **496–500**, 362–365.
27 T. Voss, C. Bekeny, L. Wischmeier, H. Gafsi, S. Borner, W. Schade, A. C. Mofor, A. Bakin and A. Waag, *Appl. Phys. Lett.*, 2006, **89**, 182107.
28 Y. C. Kong, D. P. Yu, B. Zhang, W. Fang and S. Q. Feng, *Appl. Phys. Lett.*, 2001, **78**, 407–409.
29 R. M. Martin, *Phys. Rev. B: Solid State*, 1971, **4**, 3676–3685.
30 A. Jacob, C. Parent, P. Boutinaud, G. LeFlem, J. P. Doumerc, A. Ammar, M. Elazhari and M. Elaatmani, *Solid State Commun.*, 1997, **103**, 529–532.
31 R. Gillen and J. Robertson, *Phys. Rev. B: Condens. Matter Mater. Phys.*, 2011, **84**, 035125.
32 M. N. Huda, Y. Yan, A. Walsh, S.-H. Wei and M. M. Al-Jassim, *Phys. Rev. B: Condens. Matter Mater. Phys.*, 2009, **80**, 035205.
33 R. Laskowski, N. E. Christensen, P. Blaha and B. Palanivel, *Phys. Rev. B: Condens. Matter Mater. Phys.*, 2009, **79**, 165209.
34 D. O. Scanlon and G. W. Watson, *J. Phys. Chem. Lett.*, 2010, **1**, 3195–3199.
35 J. Pellicer-Porres, A. Segura, A. S. Gilliland, A. Muñoz, P. Rodríguez-Hernández, D. Kim, M. S. Lee and T. Y. Kim, *Appl. Phys. Lett.*, 2006, **88**, 181904.
36 Z.-H. Deng, X.-D. Fang, R.-H. Tao, W.-W. Dong, S. Zhou, G. Meng and J.-Z. Shao, *J. Inorg. Mater.*, 2011, **26**, 281–285.
37 C. E. Tyner, W. D. Drotning and H. G. Drickamer, *J. Appl. Phys.*, 1976, **47**, 1044–1047.
38 P. Boutinaud, D. Garcia, C. Parent, M. Faucher and G. Leflem, *J. Phys. Chem. Solids*, 1995, **56**, 1147–1154.
39 W. Lan, W. L. Cao, M. Zhang, X. Q. Liu, Y. Y. Wang, E. Q. Xie and H. Yan, *J. Mater. Sci.*, 2009, **44**, 1594–1599.
40 Y. Wang, H. Gong, F. Zhu, L. Liu, L. Huang and A. C. H. Huan, *Mater. Sci. Eng., B*, 2001, **85**, 131–134.
41 B. J. Ingram, M. I. Bertoni, K. R. Poeppelmeier and T. O. Mason, *Thin Solid Films*, 2005, **486**, 86–93.
42 W. Lan, M. Zhang, G. B. Dong, Y. Y. Wang and H. Yan, *J. Mater. Res.*, 2007, **22**, 3338–3343.
43 J. D. Barrie, B. Dunn, G. Hollingsworth and J. I. Zink, *J. Phys. Chem.*, 1989, **93**, 3958–3963.
44 P. K. Mehrotra and R. Hoffmann, *Inorg. Chem.*, 1978, **17**, 2187–2189.
45 A. Buljan, M. Llunell, E. Ruiz and P. Alemany, *Chem. Mater.*, 2001, **13**, 338–344.
46 Z. Q. Yao, B. He, L. Zhang, C. Q. Zhuang, T. W. Ng, S. L. Liu, M. Vogel, A. Kumar, W. J. Zhang, C. S. Lee, S. T. Lee and X. Jiang, *Appl. Phys. Lett.*, 2012, **100**, 062102.
47 A. Nakanishi and H. Katayama-Yoshida, *Solid State Commun.*, 2012, **152**, 24–27.
48 A. Nakanishi and H. Katayama-Yoshida, *Solid State Commun.*, 2012, **152**, 2078–2081.
49 E. R. Ylvisaker and W. E. Pickett, *EPL*, 2013, **101**, 57006.